Biomass Conversion and Biorefinery (2023) 13:13369–13380
https://doi.org/10.1007/s13399-021-01944-6

ORIGINAL ARTICLE

Investigation on hexavalent chromium removal from simulated wastewater using royal poinciana pods-derived bioadsorbent

Arvind Singh[1] · Neha Srivastava[1] · Maulin Shah[2] · Abeer Hashem[3] · Elsayed Fathi Abd Allah[4] · Dan Bahadur Pal[5]

Received: 29 July 2021 / Revised: 1 September 2021 / Accepted: 8 September 2021 / Published online: 7 October 2021

Abstract

The biosorption capability of royal poinciana pod-derived biosorbent was investigated for the removal of hexavalent chromium from synthetic wastewater. Scanning electron microscopy, X-ray diffraction, and Fourier transform infrared spectroscopy were used to examine the morphology and other properties of the biochar prepared by pyrolysis at 350 °C. Operational parameters such as pH, biochar dose, interaction time, and starting metal ion concentration were tuned. A maximum metal removal efficiency of 93% was achieved at pH 6.0. Optimization investigations for experiments have also been conducted using response surface methodology which included three parameters by applying Box-Behnken design with 10.48 of model F-value and 0.93 of R^2 value (coefficient of determination). The kinetic theories and isotherm models of Cr (VI) ion adsorption have also been established. Pseudo-second-order model foretells the kinetics with 0.97 R^2 value. The Temkin isotherm and Dubinin-Radushkevitch provided the best-fit isotherms to explain adsorption phenomenon. This study suggests that royal poinciana pod-derived biochar may be used as an efficient, low-cost, and eco-friendly wastewater treatment bioadsorbent.

Keywords Adsorption · Chromium · Royal poinciana · Biochar · Wastewater

1 Introduction

Chromium compounds are extensively employed in various industries such as electroplating, metal extraction, magnetic tapes, paint, dyes, tannery, chemical production, semiconductor, and others [1]. The major source of chromium pollution is effluent from these plants. Chromium (VI) compounds are of major disquiet due to their high water solubility and mobility [2]. Chromate and dichromate are the most stablein nature, movable, and poisonous types of Cr (VI). Nausea, diarrhea, liver and kidney damage, rashes, internal bleeding, and respiratory difficulties are all symptoms of Cr (VI) poisoning [3]. Inhalation can result in acute poisoning, nasal septum irritation and ulceration, and respiratory sensitization (asthma) [4]. Contact with the skin can cause chronic intoxication, burn injuries, and delay the remedial of wounds and scrapes. This can progress to perforation and severe chronic allergic side effects if not treated quickly. Exposure to the eyes may result in long-term harm [5]. The necessity for low-cost technologies that can be used under local settings was highlighted by the chromium water pollution.

Various removal techniques like chemical precipitation, ion exchange, membrane and ultra-separation, sedimentation, adsorption, and other methods in the removing of chromium from water have all been reported [6–8]. Chemical precipitation has long been the most common method. The addition of a basic causes chromium hydroxide to precipitate, however this technique creates sludge. Without retrieving the metal, it transforms the water pollution problem into a solid waste disposal concern [9]. Although ion exchange is a good option, it has higher operational cost.

✉ Dan Bahadur Pal
danbahadur.chem@gmail.com

1 Department of Chemical Engineering and Technology, Indian Institute of Technology (BHU), Varanasi, India 221005

2 Chief Scientist and Head at Environmental Technology Limited, Ankeleshwar, Gujrat, India

3 Botany and Microbiology Department, College of Science, King Saud University, P.O. Box. 2460, Riyadh 11451, Saudi Arabia

4 Plant Production Department, College of Food and Agricultural Sciences, King Saud University, P.O. Box. 2460, Riyadh 11451, Saudi Arabia

5 Department of Chemical Engineering, Birla Institute of Technology, Mesra, Ranchi 835215, Jharkhand, India

Other drawbacks of these technologies include high capital and operating expenses, time consumption, careful process stages, hazardous sludge by-products, and high-tech upkeep [10].

In the case of chromium remediation, adsorption is the generally enticing technique [11, 12]. The utilization of various adsorbents such as red mud, coal, nanomaterials, industrial waste, biomass, and activated sludge-derived biosorbents for selective adsorption has piqued the interest of researchers [13]. Numerous different new adsorbents may not be applied economically in the context of industrial scale and may necessitate significant amounts of energy and reagents in their preparation. As a result, higher costs and severe environmental consequences are found [14]. Therefore, developing environmentally acceptable, low-cost, and highly efficient adsorbents are a main concern. Recently, researchers have been working on producing these optimized cost-based adsorption for the decontamination of hazardous heavy metals from water such as Cr [15, 16].

Biochar is a potential green ingredient whose sorption characteristics have been investigated for the remediation of pollutants in water [17, 18] such as chromium and other heavy metal ions. Biochar is a carbon-rich substance made by thermo-chemically converting biomass and carbonaceous materials [19]. Biochar has a greater surface area and porosity, as well as a more pronounced structure [20]. Because of its increased surface area and intensely aromatized surface with diverse functional groups, biochar has excellent adsorption properties [21]. As a low-cost and cost-effective technique to remove various pollutants, biochar is increasingly replacing activated carbon [22]. Carbon-based substances, including such wood, shell, and coal, were indeed prohibitively costly to use as raw material for industrial biochar synthesis, particularly since these materials are usually not locally available [23, 24]. Other biomass wastes were heat treated (process called pyrolysis) to produce comparative lower cost biochars [25–27]. Rapeseed stem [28] and *Melia azedarach* wood [29] have been pyrolyzed into biochar, and both have a good effect on pollutant removal. Das et al. [26] used crop, weed, and tree biomass to convert into biochar for HMs removal (Cd, Pb, Ni, Zn, Cu, As). Mokrzycki et al. [30] applied freshwater hornwort and macroalga to produce biochars in the removal of Cr ions. Biochars become more appealing, while easily accessible waste biomass materials will be used as a raw material. To find more effective and economical adsorbents, our research groups are increasingly focusing on the adsorption characteristics of biochars produced from regionally accessible royal poinciana (*Delonix regia*) pods (RPP).

In this work, the pyrolytic production of RPP pods mediated bioadsorbent at lower temperatures lacking surface functionalization was studied for the remediation of Cr (VI) metal ions from synthetic wastewater. Various process variables like as adsorbent quantity, pH, initial Cr (VI) metal ion concentration, and interaction duration were examined during the investigation. Furthermore, Fourier transform infrared spectroscopy (FTIR), X-ray diffraction (XRD), scanning electron spectroscopy (SEM), and inductively coupled plasma optical emission spectrometry (ICP-OES) were used to characterize biochar. In addition, several isotherms and theories for kinetics investigation were employed to describe the phenomena. Furthermore, response surface approach was used toward construct trials.

2 Experimental

2.1 Synthesis of biochar

Royal poinciana pods were collected from the campus of BIT Mesra Ranchi, Jharkhand, India, and cleaned with tap water to eliminate sand particles and other contaminants. After washing, the pods are dried in an oven for 48 h at a temperature of 60 °C. The dried pods are ready to be crushed and ground into powder form. The powder was stored in a sheave shaker, and all particles of similar size were separated. The larger particles were crushed again to obtain the smallest particle size. The powder sample was calcined (KF-1001 muffle furnace, Tempstar, India) at 350 °C for 3 h after all of the particles were of similar size.

2.2 Batch adsorption experiments

A self-fabricated experimental apparatus was used for batch adsorption evaluation. The experimental setup comprises of a continuous magnetic stirrer (300 rpm) and a 100-mL beaker as a reactor. Synthetic wastewater was prepared by hexavalent chromium standard solution of 0.001 g/mL. This standard was obtained from AccuStandard, Inc. Chromium-containing aqueous solutions were kept in this reactor with initial concentration range from 0.8 to 2.5 ppm. The adsorption tests were also carried out by varying the bioadsorbent dose from 20 to 80 mg. The tests were carried out for 120 min in order to optimize bioadsorbent dosage, solution pH, and heavy metal content in the aqueous solution. All experiments were performed at room temperature (303 K). Sample was taken at various time intervals. Filtration was done, and the remained chromium concentration was detected using ICP-OES, and the percentage removal efficiency was calculated. The equilibrium behavior of chromium to study the kinetics for bioadsorbent system was analyzed at optimizes conditions. The adsorption capacity of Cr (VI) by RPP biochar (q_e) was estimated using Eq. 1, and adsorption removal efficiency by RPP biochar (E %) of Cr (VI) was estimated using Eq. 2, respectively:

$$q_e = \frac{(C_{i-}C_e)V}{W} \tag{1}$$

$$\text{Adsorption efficiency E}(\%) = \frac{C_i - C_e}{C_i} \times 100 \tag{2}$$

where the volume of the solution is denoted by V (in L) and the weight of the biochar is denoted by W (in g).

2.3 Characterization

The FE-SEM image was captured on a Sigma-300 (Ametek) field emission scanning electron microscope. The prepared RPP adsorbent's Fourier transform infrared (FTIR) spectrum was obtained in the 400–4000 cm^{-1} range using a Shimadzu (Prestige 21, Japan). An X-ray diffraction (XRD) pattern was produced for phase identification using a Rigaku, Smart Lab 9 kW diffractometer (Japan), using Cu-K_α radiation at voltage of 40 kV and current of 40 mA. The Cr(VI) ion concentration and metals presented in biochar were performed using a Perkin Elmer Optical 2100 DV ICP-OES spectrometer.

2.4 Modeling and kinetics of adsorption equilibrium

The different isotherms models were used to model equilibrium relationship between q_e and Cr (VI) concentrations. The linear version of the Langmuir isotherm is as follows [31]:

$$\frac{C_e}{q_e} = \frac{1}{q_m b_o} + \frac{C_e}{q_m} \tag{3}$$

where q denotes adsorption capacity, m denotes maximum, e denotes equilibrium, and b_o denotes the Langmuir isotherm constant (in L/mg). Langmuir parameters can be derived from linear plot of Eq. 3.

The Freundlich isotherm's linearized equation can be written as [32]:

$$\ln q_e = \ln K_f + \frac{1}{n}\ln C_e \tag{4}$$

where K_f denotes the Freundlich constant and n denotes heterogeneous character. The linear plot of Eq. 4 was used to derive the constants of this isotherm.

The Temkin (Eq. 5) and D-R isotherm's (Eq. 6) linearized equation can be written as [33]:

$$q_e = \frac{\mathrm{RT}}{b_T}\ln K_T + \frac{\mathrm{RT}}{b_T}\ln C_e \tag{5}$$

$$\ln q_e = \ln q_s - \beta\epsilon^2 \tag{6}$$

where K_T (in $L.g^{-1}$) constant refers to the Temkin isotherm, b_T refers to sorption's heat (in $J.mol^{-1}$), R denotes the universal gas constant (8.314 $J.mol^{-1}.K^{-1}$), and T (in K) denotes the temperature of solution. Where s is the theoretical isotherm saturation, β (in $mol^2.k^{-1}\ J^{-2}$) is the isotherm constant. Equation 7 will be used to calculate the Polanyi potential (ε).

$$\varepsilon = \mathrm{RT}(1 + \frac{1}{C_e}) \tag{7}$$

The D-R model distinguishes between physical and chemical adsorption by calculating the E ($kJ.mol^{-1}$) free energy, necessary to eject an adsorbed species particle from its position at the binding site of adsorption to infinity. E can be calculated by using Eq. 8.

$$E = \left[\frac{1}{\sqrt{2\beta}}\right] \tag{8}$$

Various theories are present to postulate adsorption's kinetics and rate-determining steps; the pseudo-first-order (PFO) and second-order (PSO) rate theories are the most common [34]. The liner form of PFO rate model is written as follows:

$$\log\left(q_e - q_t\right) = \log q_e + \frac{k_1}{2.303}t \tag{9}$$

The linearized PSO rate expression is as follows:

$$\frac{t}{q_t} = \frac{1}{q_e^2 k_2} + \frac{t}{q_e} \tag{10}$$

Two additional kinetics models were also used to determine the kinetic mechanism. The equation for intra-particle diffusion (IPD) theory is as follows [35]:

$$q_t = t^{0.5}.k_{\mathrm{ipd}} + C \tag{11}$$

The following Eq. 12 represents the Elovich theory [36]:

$$q_t = \frac{1}{\beta}\log(\alpha\beta) + \frac{1}{\beta}\log t \tag{12}$$

whereas K_{ipd} (mg. g^{-1} min^{-1}) referred to the IPD rate constant, α denotes to adsorption and constant β denotes to processes of desorption.

2.5 Experimental design

In the current investigation, RPP has been used for preparing the biochar for the removal of heavy metal (chromium) from wastewater. The experiments were designed using the statistical analysis software Design Expert 6.0.8 to optimize

constraint and achieve the highest removal percentage under optimal conditions. For the current study, the three parameters, initial metal ion concentration, bioadsorbent dose, and pH, were taken into account. A total number of 17 experiments for the different conditions parameters (initial metal ion concentration: 1, 1.5, and 2 ppm; adsorbent dose: 40, 60, and 80 mg; and pH: 3, 6, and 9) have been performed, and the results are put into the statistical analysis. Non-linear regression analysis was used by the statistical analysis program to fit a polynomial having second-order.

3 Results and discussion

3.1 Adsorbent characterization

3.1.1 Fourier transform infrared (FTIR) analysis

The functional groups contained in the RPP biochar were identified using FTIR spectra. The observed functional groupings are depicted in Fig. 1. Because of the well-built bonding of hydrogen linked with lignin, cellulose, and pectin, a broad absorption edges for O–H stretching vibration of lignin, hemicellulose, and cellulose were observed in the 3000–3400 cm^{-1} range. Stretching of alkyle groups (C–H) has been connected to peaks found in the 3000–2700 cm^{-1} range. The band observed at 2320 cm^{-1} is associated with the aliphatic C–O groups or C≡C asymmetric stretching of hemicellulose. Peaks at 1580 cm^{-1} are ascribed to stretching of C = O. This stretching may be due to ester, ketoens, aldehydes, and hemicellulose. The bands found with 1580 cm^{-1} are associated to aromatic skeletal starch of C = C in aromatics (phenol group). The 1455 and 1405 cm^{-1} are obviously related to aromatic skeleton, C–H stretching, and ester C = C. The presence of lignin and fatty acids along with hemicellulose or cellulose may be responsible for these observed bands. The 1115 cm^{-1} band in RPP is assigned to the aromatic ring's C–O–C stretching vibration of aromatic rings related to lignin. The aromatic C–H plane bending vibration causes the 1045 and 995 cm^{-1} peak. The peak for alkenes (lignin) was observed at 869 cm^{-1}. An additional peak at 620 cm^{-1} is found in OH groups, which is attributed to O–H stretching [37–39]. Functional groups such as phenol, hydroxyl, and carboxyl are essential in pollutant adsorption via cation and anion exchange as reported in the literature [40]. The presence of functional groups such as carboxylic, phenolic, and lactonic groups on the surface of biochar helps explain its high adsorption capacity [41].

3.1.2 XRD studies

Figure 2 shows the XRD patterns biochar derived from RPP biomass pyrolyzed at 350 °C for 3 h. A number of amorphous and the crystalline phase were observed. The absence of a crystalline cellulose XRD pattern is due to pyrolysis. This observation also lends support to the biomass conversion into biochar. Observed wider peak at 24° ascribed to better layer congruence. This peak is associated to monoclinic cellulose [42, 43]. This is most likely similar to the tiny graphite structures. Because of the matching orientation of carbon coating plane, this configuration, known as a turbo-stratic, would have a 2D ordering. This apparent rise in biochar has been documented in several investigations [44, 45]. Peaks at 28.4° correspond to cristobalite (Ct). Plagioclase (PI) is associated with other peaks discovered at 29.4° and 30.9°. The xrd peak at 36°, 40.6°, and 43.3° corresponds to calcite (Cc). Furthermore, the peaks at 31.8° and

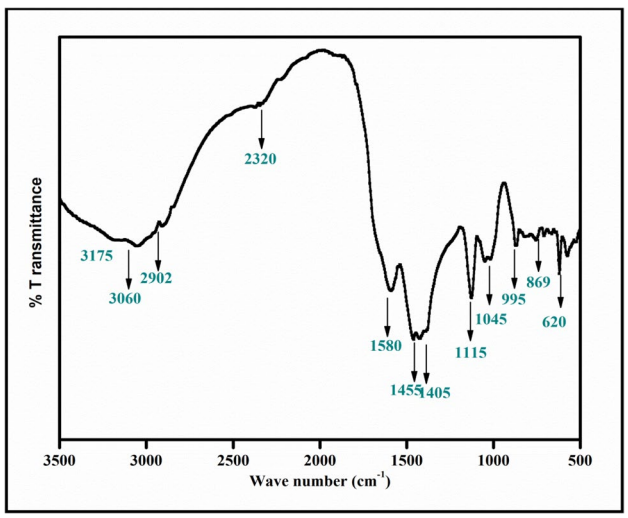

Fig. 1 FTIR spectra of royal poinciana (RP) pods-derived biochar

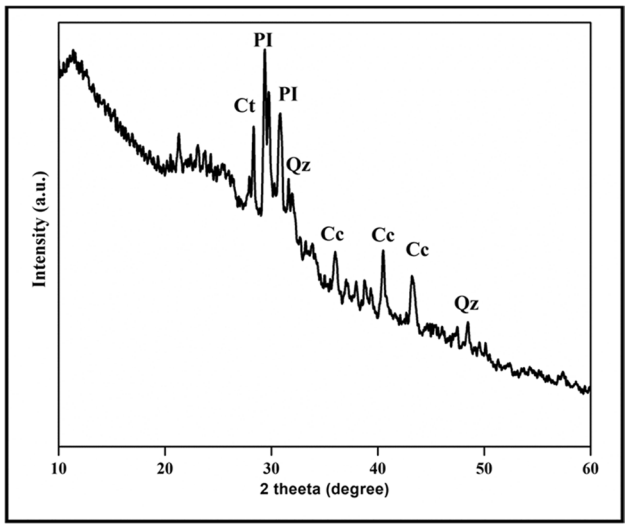

Fig. 2 XRD pattern of royal poinciana (RP) pods-derived biochar

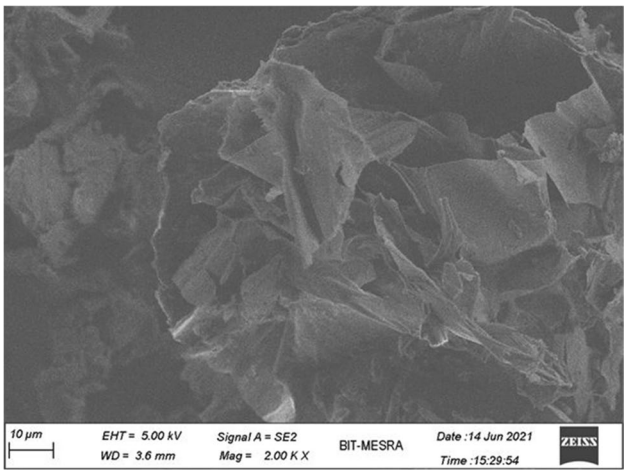

Fig. 3 FE-SEM image of royal poinciana (RP) pods-derived biochar

48.4° correspond to quartz (Qz). Minerals are responsible for these peaks seen in biochar. These peaks are because of the alkaline oxyhydroxides generated during biochar synthesis [45].

3.1.3 SEM studies and ICP analysis

The morphological study of royal poinciana pods (RPP) after 3 h of pyrolysis at 350 °C was performed using FE-SEM. Figure 3 depicts a micrograph of the bioadsorbent. The biosorbent derived from the RPP had heterogeneous structure. The biosorbents show a non-uniform morphology. Other investigations have come up with similar results. Adeniyi et al. [46] used elephant grass to make biochar. They observed a plate-like structure with a wrinkled surface. Viswanthan and coworkers [47] reported fibrous-like structures with long ridges in biochar generated from *Phragmites karka*, which resembled a pattern of parallel lines. Prior to calcination, ICP analysis of biomass revealed the presence of magnesium, iron, calcium, copper, zinc, manganese, nickel, and cobalt elements.

3.2 Statistical analysis

The chromium removal efficiency has been evaluated, and the data have been submitted to the DOE for descriptive statistics. The descriptive statistics results are presented here. The optimization research is primarily concerned with increasing the percentage of chromium removal from synthetic wastewater. To demonstrate the relevance of process parameters for percentage removal, all parameters were evaluated. and a second-order polynomial was fitted, as shown in Eq. 13. In the instance of RP pods adsorbent, Eq. 13 connects the % removal to all independent factors such as pH, adsorbent dosages, and chromium concentration (Fig. 4):

$$\begin{aligned} \%removal = &+ 51.25 + 2.416pH + 0.681CD \\ &+ 15.25C - 0.194pH^2 - 0.005CD^2 \\ &- 4.0C^2 - 0.0041pH \times CD \\ &- 0.167pH \times C - 0.05 \times CD \times C \end{aligned} \quad (13)$$

To maximize the removal %, the model equation employed three independent parameters: chromium concentration (C), adsorbent doses (CD), and pH. According to the ANOVA, the model F-value is 10.48, and the R^2 value is 0.93 with added precision 8.37, indicating that the model is relevant.

3.3 Chromium adsorption

3.3.1 Effect of contact time on chromium removal

The impact of contact time on Cr (VI) elimination was investigated for up to 120 min. (Figs. 4 and 5). The rate of metal

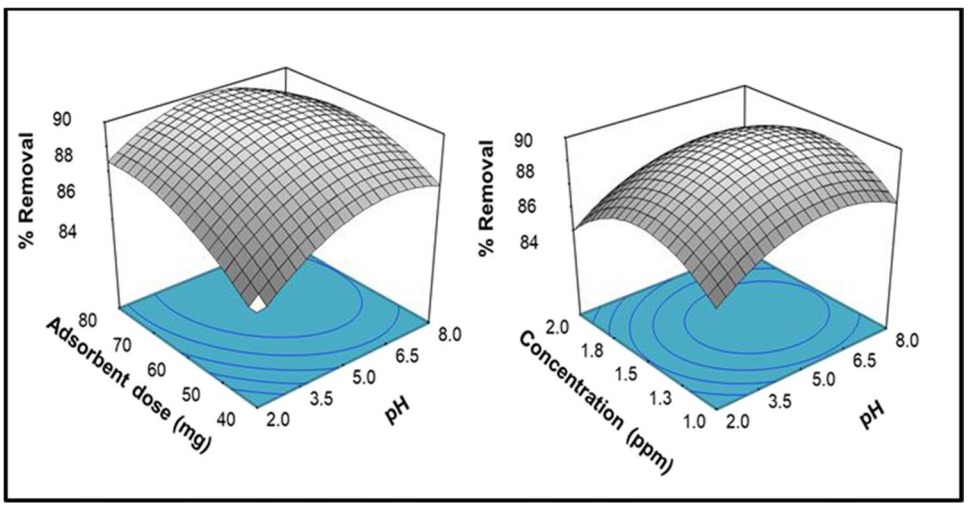

Fig. 4 RSM respone curve including effect of different parameters initial concentration of metal ions, biochar dose,and pH of solution on % Cr(VI) removal using royal poinciana (RP) pods-derived biochar

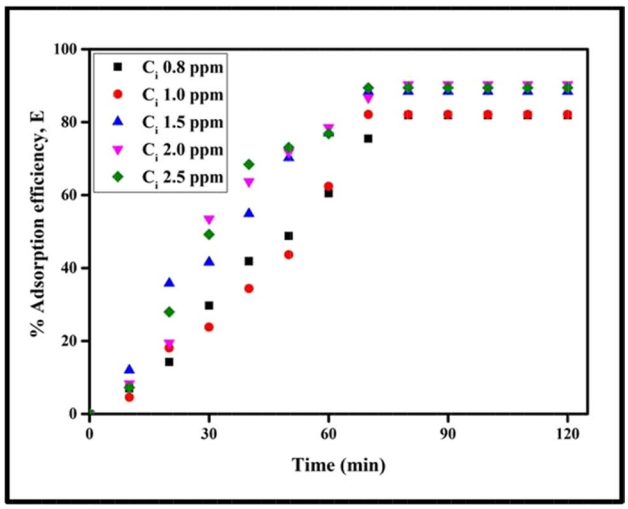

Fig. 5 Effect of contact time on Cr(VI) removal using royal poinciana (RP) pods-derived biochar adsorbent, pH = 6, adsorbent dose 0.8 g/L

ion biosorption by RPP biochar was quicker in the beginning and remained constant until reaching equilibrium (50% removal within 1 h). In a 70-min adsorption experiment, equilibrium was established. This suggests that the binding sites on the biochar either are saturated further than the steady state or that the leftover unoccupied receptors on the biochar are thorny to fill due to repulsion between both the solutes of the solid and solution. Metal ion sorption on the adsorbate is determined by the availability of binding sites and their electrostatic interaction [48, 49].

3.3.2 Effect of pH

Figures 4 and 6 depict the Cr (VI) removal efficiency of RPP biochar at various pH levels. The results demonstrate that at pH levels ranging from 3 to 6, the Cr (VI) removal efficiencies remained high, and the Cr (VI) in acidic and neutral solutions could be effectively removed. The removal efficiencies of Cr (VI) reduced when the pH rose to alkaline conditions (80.4% at pH 11). As a result, it was postulated that acidic conditions may be more suitable for Cr(VI) removal by RPP biochar. At pH 6.0, the greatest adsorption of Cr (VI) species was found on biochar adsorbent (91.3%). Cr (VI) exists in numerous stable forms, including CrO_4^{2-}, $HCrO_4^{2-}$, $Cr_2O_7^{2-}$, and $HCr_2O_7^{2-}$. Furthermore, chromium ion concentration and pH influence the comparative prevalence of a particular complex. Because of surface group's ionization, biochar is positively charged at acidic pH. The dichromate ions in sorbates, on the other hand, are negative, as a result electrostatic interaction in between sites of biochar and the sorbate [50]. Therefore, at acidic pH, it leads to enhanced adsorption. As the value of pH rises toward the alkaline range, the biosorbent deprotonates, and its capacity of adsorption diminishes. As a result, all future investigations were conducted at pH 6.0. Similar findings on other adsorbents have been reported, previously [51, 52]. Ahmadi et al. (2016) stated [53] that at pH 8.1, the increase of competition with more OH ions hindered the movement of Cr (VI) ions towards biochar. These findings suggest that electrostatic interaction is more significant in Cr (VI) adsorption in an acidic solution, whereas ion exchange is more relevant in an alkaline solution.

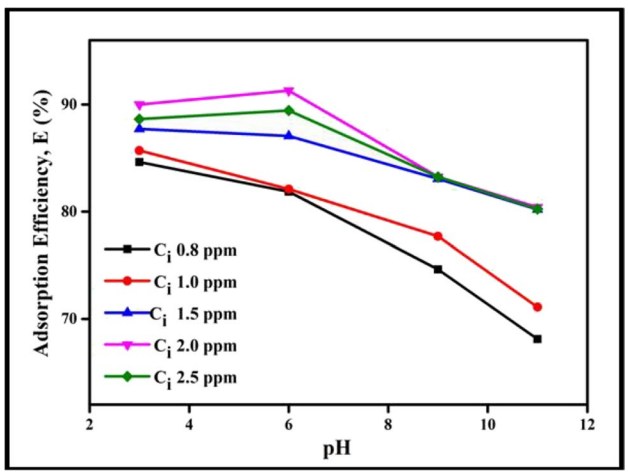

Fig. 6 Effect of pH on Cr(VI) removal using royal poinciana (RP) pods-derived biochar adsorbent, adsorbent dose 0.8 g/L

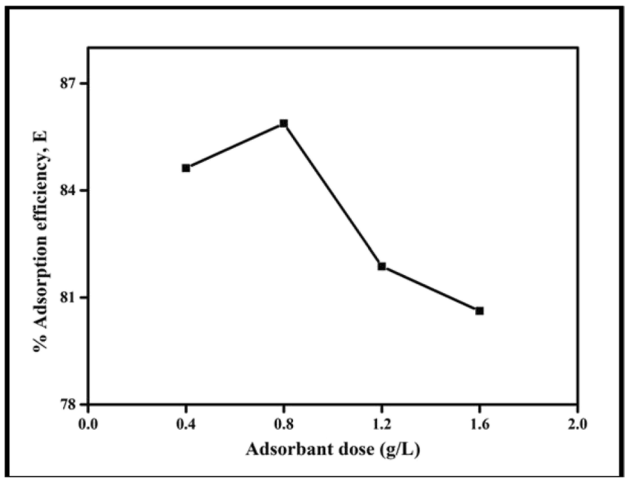

Fig. 7 Effect of adsorbent dose on Cr(VI) removal, pH = 6, C_i = 0.8 ppm

3.3.3 Effect of biochar dose

The adsorbent dose is regarded as an important parameter that can influence the adsorption process [54]. Figures 4 and 7 depict the findings of Cr (VI) adsorption by RPP biochar at various dosages. The removal efficiency improved when the adsorbent dose was increased. Adsorption removal efficiency improved from 84.6 to 85.9% when the biochar dose was raised from 0.4 to 0.8 g/L. The biochar adsorption efficiency of removal decreased significantly at 1.2 g/L and 1.6 g/L of adsorbent, reaching 80.6%. As a result, the biochar dose of 0.8 g/L was chosen for the adsorption tests. The decline can be attributed to the splitting phenomena of the concentration gradient [55].

3.3.4 Effect of Cr (VI) initial concentration

The removal efficiency increased from 81.8 to 91.3% as the Cr (VI) ion content increased from 0.8 to 2 mg/L (Figs. 4 and 8). Following that, the rise in Cr (VI) removal efficiency decreased when the concentration of Cr (VI) content kept at 2 and 2.5 mg/L. This reduction in removal effectiveness might be ascribed to the biochar's restricted limited count of active sites for binding. While concentration of metal Cr (VI) ions was increased, saturation level of the biochar surface adsorption capacity was achieved and therefore not capable to remove any more Cr (VI), resulting in a reduction in Cr(VI) migration in transportation to the biochar surface from the solution [56]. Furthermore, when the Cr (VI) content rose, a new layer (adsorbed Cr ions) developed on the biochar surface. This reduced the effectiveness of biochar removal even further and hampered the combination of Cr (VI) with biochar [57].

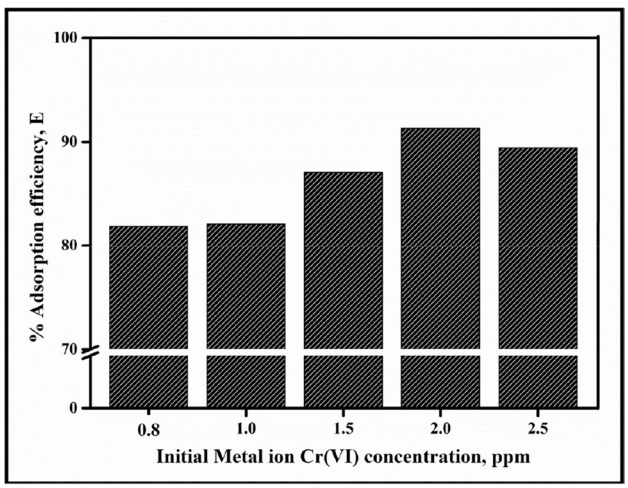

Fig. 8 Effect of initial metal Cr(VI) ion concentrations on Cr(VI) removal, pH = 6, adsorbent dose 0.8 g/L

3.4 Isotherm modelling

The Temkin isotherm provided the best fit ($R^2 = 0.99$) of all isotherm models tested (Fig. 9). According to this model, the heat adsorption of a solute in a layer decreases proportionally with surface cover-up due to adsorbent metal interactions, where metal adsorption is specified by a uniform binding affinity distribution. The existence of b_T value larger than zero suggests that the adsorption Cr (VI) metal on RPP biochar process is likely to be exothermic [58]. As a result, electrostatic association was one of the processes involved in metal adsorption on biochar. The outcome was consistent with the previous reported pH impact discussion. The D-R isotherm ($R^2 = 0.98$) presumes that biosorption is a consequence of the porous property of the adsorbent. It is primarily applied to distinguish physical and chemical phenomenon-based adsorption. The calculated value of E is 2.39 kJ. mol^{-1} (Table 1) indicates the physical nature of Cr (VI) biosorption on RPP biochar and the involvement of Van-der Waals forces.

The Langmuir theory has assumption that monolayer adsorption of metal ions happens at a specific amount of homogeneous dispersion active sites over the surface of adsorbent at equilibrium; moreover, those binding sites have identical attraction for the sorbate. The Freundlich theory has assumption that the biosorption phenomenon on a heterogeneous surface comes as a result of multi-layers with varying affinity for the adsorbate. However, lower correlation values were obtained for the Freundlich ($R^2 = 0.97$) and Langmuir ($R^2 = 0.95$) models than with the others, implying that these models were not acceptable. Similar findings have been seen in other studies in adsorption of pollutants on different biochars [59–61]. For Cr(VI) removal, Khalil et al. [59] employed biochar made from tea waste and rice husk. The adsorption isotherms were described using the Temkin and D-R models. Amin et al. [60] reported on another study that used biochar produced from orange peel to remove Cd(II). For equilibrium data, the Temkin and D-R isotherm models had the highest correlation factor. Meng and his coworkers' [61] research on wastewater treatment with biochar generated from cotton shell was well explained by the Temkin model. According to calculations, the Langmuir isotherm constant (R_L) for RPP biochar is 0.2988 (Table 1). It was postulated that the biochars' surface adsorption of the Cr metal ion was beneficial because R_L was less than 1 [62].

3.5 Kinetic studies

Adsorption kinetics is the study to relate solute absorption rate at the phase boundaries. To evaluate the kinetics of chromium adsorption, adsorption data from RPP biochar under optimum conditions were analyzed using PFO, PDO, Elovich, and IPD kinetic models. Table 2 contains

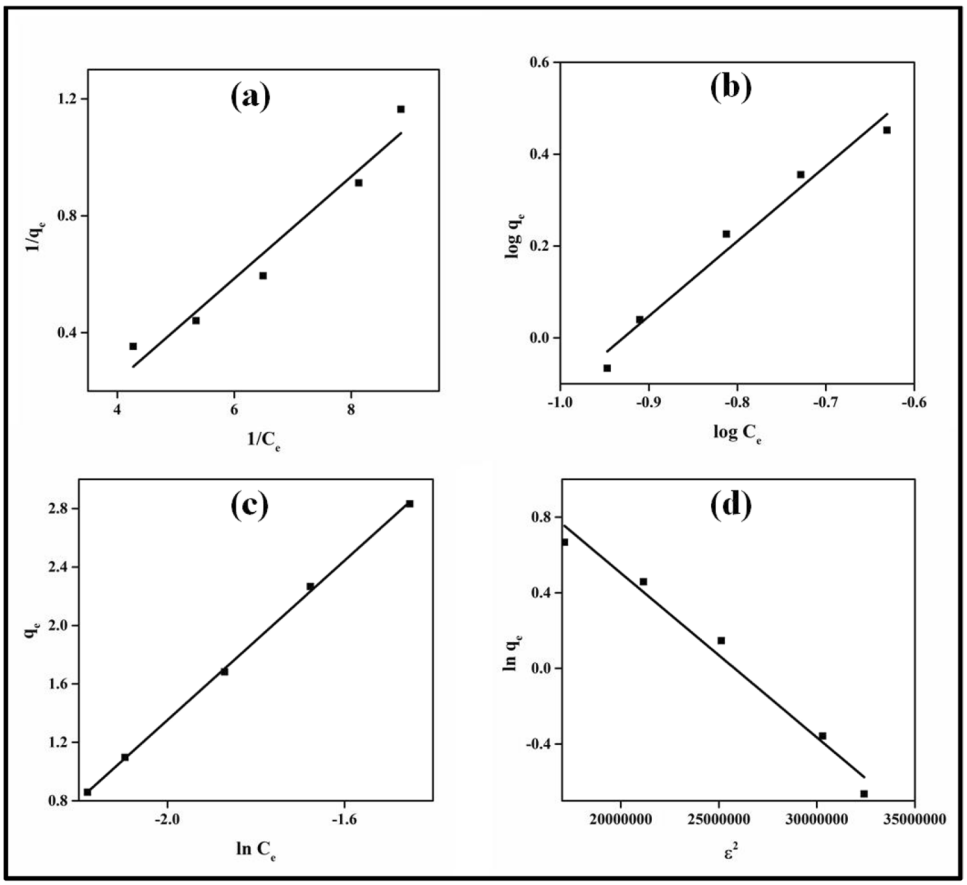

Fig. 9 Isotherm study of Cr(VI) removal on the biochar adsorbent of royal poinciana (RP) pods (**a**) Langmuir, (**b**) Freundlich, (**c**) Temkin, and (**d**) D-R model

the value of kinetic parameters. Figure 10 depicts the linearized form of all kinetics theories. In the PFO kinetic model, the R^2 value for linear plot between log (q_e–q) vs. time is observed to 0.93 (Fig. 10a). The value of R^2 is found to be 0.97 in the case of PSO kinetic theory. The PSO rate constant K_2 and adsorption capacity were calculated from the slope and intercept of plots drawn between t/q_t and t. These parameters are depicted in Table 2. PSO

Table 1 Equilibrium parameters of Cr(VI) adsorption on the royal poinciana pod-derived biochars (RPP)

Isotherm model	Parameters	Value
Langmuir	q_m (mg.g^{-1})	2.15
	K_L (L.mg^{-1})	2.66
	R_L	0.215
	R^2	0.95
Freundlich	K_F (L.mg^{-1})	33.113
	1/n	1.63
	R^2	0.97
Temkin	B_T (J.mol^{-1})	1360
	K_T (L.mg^{-1})	12.12
	R^2	0.999
D-R	q_m (mg.g^{-1})	9.42
	β (mol^2.kJ^{-2})	9.39E-08
	E_a (kJ.mol^{-1})	2.39
	R^2	0.98

Table 2 Kinetic parameters of Cr(VI) adsorption on royal poinciana pod-derived biochars (RPP)

Kinetic model	Parameters	Value
Pseudo-first-order	$q_{e,\,cal}$ (mg.g^{-1})	1.27
	k_1 (min^{-1})	0.055
	R^2	0.93
Pseudo-second-order	$q_{e,\,cal}$ (mg.g^{-1})	1.58
	k_2 (g/mg.min)	0.058
	R^2	0.97
Intra-particle diffusion		
1st region	$k_{d,1}$ (mg.g^{-1}min$^{1/2}$)	0.48
	C_1	1.39
	R^2	0.88
2nd region	$k_{d,2}$ (mg.g^{-1}min$^{1/2}$)	0.245
	C_2	0.0116
	R^2	0.97
Elovich	α	1.005
	B	0.397
	R^2	0.93

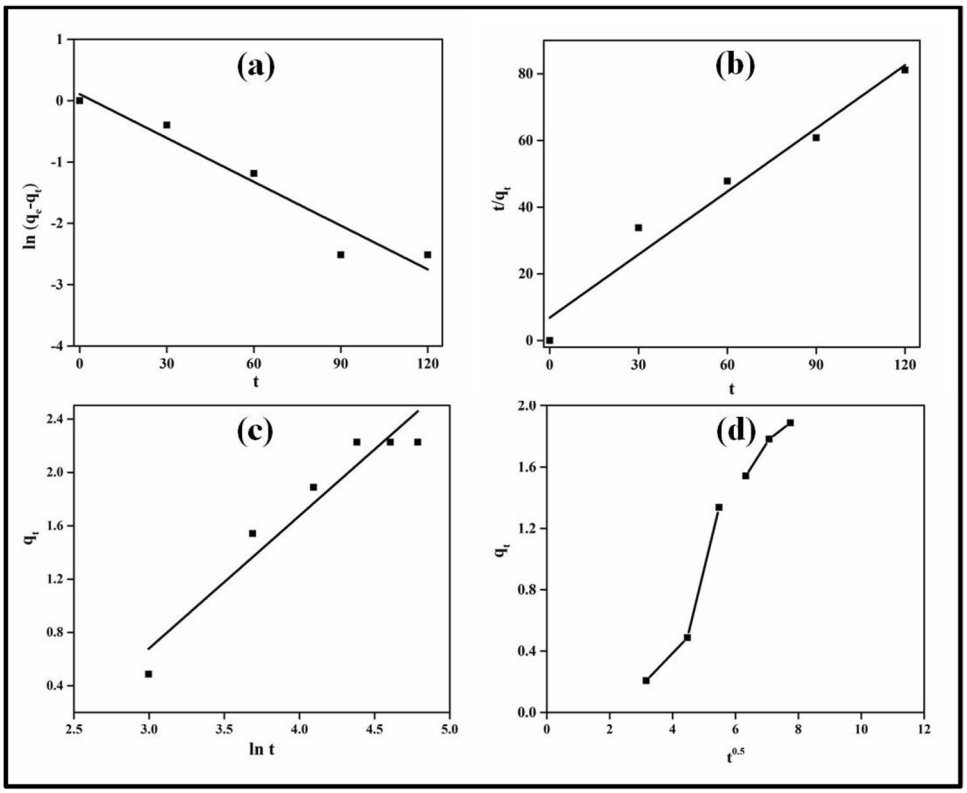

Fig. 10 Kinetic study of adsorption of Cr(VI) metal ions on the biochar adsorbent of royal poinciana (RP) pods (**a**) pseudo-first-order, (**b**) pseudo-second-order, (**c**) Elovich model, and (**d**) intra-particle diffusion model

hypothesis is well suited to describe the kinetics of Cr (VI) adsorption onto biochar derived from RP pods.

Furthermore, the porous character of the biosorbent might involve possible metal remediation by the many steps process typically ruled by three separate mechanisms [63]: First, transportation of metal from solution to the biosorbent surface through film diffusion; second, diffusion of metal ions inside the biosorbent pore surface area; and finally biosorption of metal ions inside biosorbent pores. Thus, experimental kinetic data were analyzed using IPD kinetic theory to foretell the adsorption process of metal Cr (VI) by RPP biochar and to find the rate deciding step. The assumption of this IPD is that if the intercept is 0, that is, if the linear plot of qt vs. $t^{0.5}$ (Fig. 10d) passes through the (0,0) Cartesian coordinates, then IPD will be the sole rate-limiting step. The plot for IPD theory did not pass through the (0,0) Cartesian coordinates (origin), implying that the external adsorption may control Cr (VI) remediation process on RPP biochar [64]. The pattern of the IPD plot (Fig. 10d) indicates multi-linear steps (three phases), showing that IPD is not the only rate-limiting step, as the model assumes. Furthermore, the first part represents surface adsorption (film diffusion), which occurs when Cr(VI) diffuses through the solution on the surface of RPP-derived biochar. The next portion shows progressive sorption towards equilibrium. The final uninterrupted plots showed the final equilibrium stage, during which IPD was further decreased due to very low metal ion concentrations left in the system. IPD graph for metal Cr(VI) ion adsorption derived from Bermuda grass shows similar multi-linearity [65]. Another research on the removal of aqueous Cr(VI) by magnetic biochar derived from *Melia azedarach* wood biomass found a multi-stage linearity in the intra-particle diffusion plot [29]. The Elovich model expresses the heterogeneous diffusion process, which is regulated by the response rate with diffusion coefficient. Correlation factor is low for Elovich theory, i.e., 0.92. Therefore, no postulation can be made (Fig. 10c, Table 2).

FTIR spectrum data (Fig. 1) were utilized to better understand the biosorption mechanism of Cr(VI) metal ion removal on RPP produced biochar. As per the FTIR band, the mainly functional groups discovered on RPP generated biochar are –OH groups. This hypothesis proposed that metal ions could be aligned to the –OH groups present on the RPP surface.

4 Conclusion

In this paper, royal poinciana pods-derived biochars were employed in the removal of Cr (VI) from aqueous solution. Equilibrium was achieved within 70 min. Maximum 91.3% removal efficiency for Cr (VI) was attained at the optimal pH of 6.0. The pseudo-second-order model ($R^2 > 0.97$) accurately characterized the Cr (VI) sorption process. The

Temkin model ($R^2 > 0.99$) and the Dubinin-Radushkevitch model ($R^2 > 0.98$) were used to described the sorption equilibrium data. FTIR studies revealed that biochar has abundant various functional groups including hydroxyl and other oxygen-containing groups. XRD analysis indicated that certain beneficial additional types of minerals were present in the biochar. Based on our findings, royal poinciana pods-derived biochar might be a viable option for removing hazardous Cr (VI) in wastewater treatment.

Acknowledgements The authors thankfully acknowledge Birla Institute of Technology, Mesra, Ranchi, Jharkhand, and IIT (BHU), Varanasi, for characterization of the materials. DBP is thankful to NPIU (TEQIP-III), Govt. of India for the financial support. The authors would like to extend their sincere appreciation to the Researchers Supporting Project Number (RSP-2021/356), King Saud University, Riyadh, Saudi Arabia.

Declarations

Conflict of interest The authors declare no competing interests.

References

1. Jin W, Du H, Zheng S, Zhang Y (2016) Electrochemical processes for the environmental remediation of toxic Cr(VI): a review. Electrochim Acta 191:1044–1055. https://doi.org/10.1016/j.electacta.2016.01.130
2. Rakhunde R, Deshpande L, Juneja HD (2012) Chemical speciation of chromium in water: a review. Crit Rev Environ Sci Technol 42:776–810. https://doi.org/10.1080/10643389.2010.534029
3. Prasad S, Yadav KK, Kumar S, Gupta N, Cabral-Pinto MMS, Rezania S et al (2021) Chromium contamination and effect on environmental health and its remediation: a sustainable approaches. J Environ Manag 285:112174. https://doi.org/10.1016/j.jenvman.2021.112174
4. Browning CL, Wise JP (2017) Prolonged exposure to particulate chromate inhibits RAD51 nuclear import mediator proteins. Toxicol Appl Pharmacol 331:101–107. https://doi.org/10.1016/j.taap.2017.05.030
5. Cefalu WT, Hu FB (2004) Role of chromium in human health and in diabetes. Diabetes Care 27:2741–2751. https://doi.org/10.2337/diacare.27.11.2741
6. Fu F, Wang Q (2011) Removal of heavy metal ions from wastewaters: a review. J Environ Manag 92:407–418. https://doi.org/10.1016/j.jenvman.2010.11.011
7. GracePavithra K, Jaikumar V, Kumar PS, SundarRajan P (2019) A review on cleaner strategies for chromium industrial wastewater: present research and future perspective. J Cleaner Prod 228:580–593. https://doi.org/10.1016/j.jclepro.2019.04.117
8. Almeida JC, Cardoso CED, Tavares DS, Freitas R, Trindade T, Vale C et al (2019) Chromium removal from contaminated waters using nanomaterials –a review. TrAC Trends Anal Chem 118:277–291. https://doi.org/10.1016/j.trac.2019.05.005
9. Chen Q, Yao Y, Li X, Lu J, Zhou J, Huang Z (2018) Comparison of heavy metal removals from aqueous solutions by chemical precipitation and characteristics of precipitates. J Water Process Eng 26:289–300. https://doi.org/10.1016/j.jwpe.2018.11.003
10. Keng P-S, Lee S-L, Ha S-T, Hung Y-T, Ong S-T (2014) Removal of hazardous heavy metals from aqueous environment by low-cost adsorption materials. Environ Chem Lett 12:15–25. https://doi.org/10.1007/s10311-013-0427-1
11. Islam MA, Angove MJ, Morton DW (2019) Recent innovative research on chromium (VI) adsorption mechanism. Environ Nanotechnol Monit Manag 12:100267. https://doi.org/10.1016/j.enmm.2019.100267
12. Miretzky P, Cirelli AF (2010) Cr(VI) and Cr(III) removal from aqueous solution by raw and modified lignocellulosic materials: a review. J Hazard Mater 180:1–19. https://doi.org/10.1016/j.jhazmat.2010.04.060
13. Saleem J, Shahid UB, Hijab M, Mackey H, McKay G (2019) Production and applications of activated carbons as adsorbents from olive stones. Biomass Conv Bioref 9:775–802. https://doi.org/10.1007/s13399-019-00473-7
14. Kumar R, Laskar MA, Hewaidy IF, Barakat MA (2019) Modified adsorbents for removal of heavy metals from aqueous environment: a review. Earth Syst Environ 3:83–93. https://doi.org/10.1007/s41748-018-0085-3
15. Chakraborty R, Asthana A, Singh AK, Jain B, Susan ABH (2020) Adsorption of heavy metal ions by various low-cost adsorbents: a review. Int J Environ Anal Chem 1-38. https://doi.org/10.1080/03067319.2020.1722811
16. Malik DS, Jain CK, Yadav AK (2017) Removal of heavy metals from emerging cellulosic low-cost adsorbents: a review. Appl Water Sci 7:2113–2136. https://doi.org/10.1007/s13201-016-0401-8
17. Das SK, Ghosh GK, Avasthe R (2020) Valorizing biomass to engineered biochar and its impact on soil, plant, water, and microbial dynamics: a review. Biomass Conv Bioref. https://doi.org/10.1007/s13399-020-00836-5
18. Gupta S, Sireesha S, Sreedhar I, Patel CM, Anitha KL (2020) Latest trends in heavy metal removal from wastewater by biochar based sorbents. J Water Process Eng 38:101561. https://doi.org/10.1016/j.jwpe.2020.101561
19. Chi NTL, Anto S, Ahamed TS, Kumar SS, Shanmugam S, Samuel MS et al (2021) A review on biochar production techniques and biochar based catalyst for biofuel production from algae. Fuel 287:119411. https://doi.org/10.1016/j.fuel.2020.119411
20. Inyang MI, Gao B, Yao Y, Xue Y, Zimmerman A, Mosa A, Pullammanappallil P, Ok YS, Cao X (2016) A review of biochars as a low-cost adsorbent for aqueous heavy metal removal. Crit Rev Environ Sci Technol 46:406–433. https://doi.org/10.1080/10643389.2015.1096880
21. Song J, He Q, Hu X, Zhang W, Wang C, Chen R et al (2019) Highly efficient removal of Cr(VI) and Cu(II) by biochar derived from *Artemisia argyi* stem. Environ Sci Pollut Res 26:13221–13234. https://doi.org/10.1007/s11356-019-04863-2
22. Oliveira FR, Patel AK, Jaisi DP, Adhikari S, Lu H, Khanal SK (2017) Environmental application of biochar: current status and perspectives. Bioresour Technol 246:110–122. https://doi.org/10.1016/j.biortech.2017.08.122
23. Qiu B, Tao X, Wang H, Li W, Ding X, Chu H (2021) Biochar as a low-cost adsorbent for aqueous heavy metal removal: a review. J Anal Appl Pyrolysis 155:105081. https://doi.org/10.1080/10643389.2015.1096880
24. Das SK, Ghosh GK, Avasthe R (2020) Biochar application for environmental management and toxic pollutant remediation. Biomass Conv Bioref. https://doi.org/10.1007/s13399-020-01078-1
25. Li Y, Xing B, Ding Y, Han X, Wang S (2020) A critical review of the production and advanced utilization of biochar via selective pyrolysis of lignocellulosic biomass. Bioresour Technol 312:123614. https://doi.org/10.1016/j.biortech.2020.123614
26. Das SK, Ghosh GK, Avasthe R (2021) Conversion of crop, weed and tree biomass into biochar for heavy metal removal and wastewater treatment. Biomass Conv Bioref. https://doi.org/10.1007/s13399-021-01334-y

27. Gupta GK, Mondal MK (2020) Mechanism of Cr(VI) uptake onto sagwan sawdust derived biochar and statistical optimization via response surface methodology. Biomass Conv Bioref. https://doi.org/10.1007/s13399-020-01082-5
28. Zhao B, O'Connor D, Zhang J, Peng T, Shen Z, Tsang DCW, Hou D (2018) Effect of pyrolysis temperature, heating rate, and residence time on rapeseed stem derived biochar. J Clean Prod 174:977–987. https://doi.org/10.1016/j.jclepro.2017.11.013
29. Zhang X, Lv L, Qin Y, Xu M, Jia X, Chen Z (2018) Removal of aqueous Cr(VI) by a magnetic biochar derived from Melia azedarach wood. Bioresour Technol 256:1–10. https://doi.org/10.1016/j.biortech.2018.01.145
30. Mokrzycki J, Michalak I, Rutkowski P (2021) Biochars obtained from freshwater biomass—green macroalga and hornwort as Cr(III) ions sorbents. Biomass Conv Bioref 11:301–313. https://doi.org/10.1007/s13399-020-00649-6
31. Amaku JF, Nnaji JC, Ogundare SA, Akpomie KG, Ngwu CM, Chukwuemeka-Okorie HO et al (2021) Chrysophyllum albidum stem bark extract coated tillite adsorbent for the uptake of Cr(VI): thermodynamic, kinetic, isotherm, and reusability. Biomass Conv Bioref. https://doi.org/10.1007/s13399-021-01489-8
32. Show S, Karmakar B, Halder G (2020) Sorptive uptake of anti-inflammatory drug ibuprofen by waste biomass–derived biochar: experimental and statistical analysis. Biomass Conv Bioref. https://doi.org/10.1007/s13399-020-00922-8
33. Motejadded Emrooz HB, Maleki M, Rashidi A, Shokouhimehr M (2021) Adsorption mechanism of a cationic dye on a biomass-derived micro- and mesoporous carbon: structural, kinetic, and equilibrium insight. Biomass Conv Bioref 11:943–954. https://doi.org/10.1007/s13399-019-00584-1
34. Cheng C, Jia M, Cui L, Li Y, Xu L, Jin X (2020) Adsorption of Cr(VI) ion on tannic acid/graphene oxide composite aerogel: kinetics, equilibrium, and thermodynamics studies. Biomass Conv Bioref. https://doi.org/10.1007/s13399-020-00899-4
35. Jain SN, Tamboli SR, Sutar DS, Jadhav SR, Marathe JV, Mawal VN (2020) Kinetic, equilibrium, thermodynamic, and desorption studies for sequestration of acid dye using waste biomass as sustainable adsorbents. Biomass Conv Bioref. https://doi.org/10.1007/s13399-020-00780-4
36. Machado Garcia R, Carleer R, Arada Pérez M, Gryglewicz G, Maggen J, Haeldermans T et al (2020) Adsorption of Cibacron Yellow F-4G dye onto activated carbons obtained from peanut hull and rice husk: kinetics and equilibrium studies. Biomass Conv Bioref. https://doi.org/10.1007/s13399-020-00699-w
37. Chia CH, Gong B, Joseph SD, Marjo CE, Munroe P, Rich AM (2012) Imaging of mineral-enriched biochar by FTIR, Raman and SEM–EDX. Vib Spectrosc 62:248–257. https://doi.org/10.1016/j.vibspec.2012.06.006
38. Zhang Y, Ma Z, Zhang Q, Wang J, Ma Q, Yang Y, Luo X, Zhang W (2017) Comparison of the physicochemical characteristics of bio-char pyrolyzed from moso bamboo and rice husk with different pyrolysis temperatures. Bio Resources. 12:4652–4669. https://doi.org/10.15376/biores.12.3.4652-4669
39. Armynah B, Tahir D, Tandilayuk M, Djafar Z, Piarah WH (2019) Potentials of biochars derived from bamboo leaf biomass as energy sources: effect of temperature and time of heating. Int J Biomater. https://doi.org/10.1155/2019/3526145
40. Sun Y, He Y, Tang B, Wu Z, Tao C, Ban J et al (2018) Selective adsorption and decomposition of pollutants using RGO-TiO2 with optimized surface functional groups. RSC Adv 8:31996–32002. https://doi.org/10.1039/C8RA05345F
41. Sahu S, Pahi S, Tripathy S, Singh SK, Behera A, Sahu UK et al (2020) Adsorption of methylene blue on chemically modified lychee seed biochar: dynamic, equilibrium, and thermodynamic study. J Mol Liq 315:113743. https://doi.org/10.1016/j.molliq.2020.113743
42. Veiga PAdS, Schultz J, Matos TTdS, Fornari MR, Costa TG, Meurer L, Mangrich AS (2020) Production of high-performance biochar using a simple and low-cost method: optimization of pyrolysis parameters and evaluation for water treatment. J Anal Appl Pyrolysis 148:104823. https://doi.org/10.1016/j.jaap.2020.104823
43. Ighalo JO and Adeniyi AG (2021) Statistical modelling and optimisation of the biosorption of Cd(II) and Pb(II) onto dead biomass of Pseudomonas Aeruginosa, Chem Prod Process Model, 16. https://doi.org/10.1515/cppm-2019-0139
44. Verma L, Singh J (2019) Synthesis of novel biochar from waste plant litter biomass for the removal of arsenic (III and V) from aqueous solution: a mechanism characterization, kinetics and thermodynamics. J Environ Manag 248:109235. https://doi.org/10.1016/j.jenvman.2019.07.006
45. Mohanty P, Nanda S, Pant KK, Naik S, Kozinski JA, Dalai AK (2013) Evaluation of the physiochemical development of biochars obtained from pyrolysis of wheat straw, timothy grass and pinewood: effects of heating rate. J Anal Appl Pyrolysis 104:485–493. https://doi.org/10.1016/j.jaap.2013.05.022
46. Adeniyi AG, Ighalo JO, Onifade DV (2019) Production of biochar from elephant grass (Pernisetum purpureum) using an updraft biomass gasifier with retort heating, biofuels, 1–8. https://doi.org/10.1080/17597269.2019.1613751
47. Viswanthan SP, Neelamury SP, Parakkuzhiyil S, Njazhakunnathu GV, Sebastian A, Padmakumar B, Ambatt TP (2020) Removal efficiency of methylene blue from aqueous medium using biochar derived from Phragmites karka, a highly invasive wetland weed. Biomass Conv Bioref. https://doi.org/10.1007/s13399-020-00877-w
48. Mokrzycki J, Michalak I, Rutkowski P (2021) Biochars obtained from freshwater biomass-green macroalga and hornwort as Cr(III) ions sorbents. Biomass Conv Bioref 11:301–313. https://doi.org/10.1007/s13399-020-00649-6
49. Michalak I, Baśladyńska S, Mokrzycki J, Rutkowski P (2019) Biochar from a freshwater macroalga as a potential biosorbent for wastewater treatment. Water 11:1390. https://doi.org/10.3390/w11071390
50. Zhang L, Niu W, Sun J, Zhou Q (2020) Efficient removal of Cr(VI) from water by the uniform fiber ball loaded with polypyrrole: static adsorption, dynamic adsorption and mechanism studies. Chemosphere 248:126102. https://doi.org/10.1016/j.chemosphere.2020.126102
51. Dong H, Deng J, Xie Y, Zhang C, Jiang Z, Cheng Y et al (2017) Stabilization of nanoscale zero-valent iron (nZVI) with modified biochar for Cr(VI) removal from aqueous solution. J Hazard Mater 332:79–86. https://doi.org/10.1016/j.jhazmat.2017.03.002
52. Shakya A, Agarwal T (2019) Removal of Cr(VI) from water using pineapple peel derived biochars: adsorption potential and re-usability assessment. J Mol Liq 293:111497. https://doi.org/10.1016/j.molliq.2019.111497
53. Ahmadi M, Kouhgardi E, Ramavandi B (2016) Physico-chemical study of dew melon peel biochar for chromium attenuation from simulated and actual wastewaters. Korean J Chem Eng 33:2589–2601. https://doi.org/10.1007/s11814-016-0135-1
54. Nguyen LH, Nguyen TMP, Van HT, Vu XH, Ha TLA, Nguyen THV et al (2019) Treatment of hexavalent chromium contaminated wastewater using activated carbon derived from coconut shell loaded by silver nanoparticles: batch experiment. Water, Air, & Soil Pollut 230:68. https://doi.org/10.1007/s11270-019-4119-8
55. Hoang LP, Van HT, Nguyen LH, Mac D-H, Vu TT, Ha LT et al (2019) Removal of Cr(vi) from aqueous solution using magnetic modified biochar derived from raw corncob. New J Chem 43:18663–18672. https://doi.org/10.1039/C9NJ02661D
56. Akram M, Bhatti HN, Iqbal M, Noreen S, Sadaf S (2017) Biocomposite efficiency for Cr(VI) adsorption: kinetic, equilibrium and

thermodynamics studies. J Environ Chem Eng 5:400–411. https://doi.org/10.1016/j.jece.2016.12.002
57. Hariharan A, Harini V, Sandhya S, Rangabhashiyam S (2020) Waste Musa acuminata residue as a potential biosorbent for the removal of hexavalent chromium from synthetic wastewater. Biomass Conv Bioref. https://doi.org/10.1007/s13399-020-01173-3
58. Danish M, Ahmad T, Majeed S, Ahmad M, Ziyang L, Pin Z et al (2018) Use of banana trunk waste as activated carbon in scavenging methylene blue dye: kinetic, thermodynamic, and isotherm studies. Bioresour Technol Rep 3:127–137. https://doi.org/10.1016/j.biteb.2018.07.007
59. Khalil U, Shakoor MB, Ali S, Rizwan M, Alyemeni MN, Wijaya L (2020) Adsorption-reduction performance of tea waste and rice husk biochars for Cr (VI) elimination from wastewater. J Saudi Chem Soc 24(11):799–810
60. Amin MT, Alazba AA, Shafiq M (2019) Application of the biochar derived from orange peel for effective biosorption of copper and cadmium in batch studies: isotherm models and kinetic studies. Arab J Geosci 12:46. https://doi.org/10.1007/s12517-018-4184-0
61. Meng Q, Zhang Y, Meng D, Liu X, Zhang Z, Gao P, Lin A, Hou L (2020) Removal of sulfadiazine from aqueous solution by in-situ activated biochar derived from cotton shell. Environ Res 191:110104. https://doi.org/10.1016/j.envres.2020.110104
62. Zheng C, Zheng H, Wang Y, Wang Y, Qu W, An Q et al (2018) Synthesis of novel modified magnetic chitosan particles and their adsorption performance toward Cr(VI). Bioresour Technol 267:1–8. https://doi.org/10.1016/j.biortech.2018.06.113
63. Dong Y, Gao M, Song Z, Qiu W (2019) Adsorption mechanism of As(III) on polytetrafluoroethylene particles of different size. Environ Poll 254:112950. https://doi.org/10.1016/j.envpol.2019.07.118
64. Pholosi A, Naidoo EB, Ofomaja AE (2020) Intraparticle diffusion of Cr(VI) through biomass and magnetite coated biomass: a comparative kinetic and diffusion study. S Afr J Chem Eng 32:39–55. https://doi.org/10.1016/j.sajce.2020.01.005
65. Tu B, Wen R, Wang K, Cheng Y, Deng Y, Cao W et al (2020) Efficient removal of aqueous hexavalent chromium by activated carbon derived from Bermuda grass. J Colloid Interface Sci 560:649–658. https://doi.org/10.1016/j.jcis.2019.10.103